Anomaly detection for drilling tools based on operating mode recognition and interval-augmented Mahalanobis distance

Wenkai Hu[a,b,c], Bin Hu[a,b,c], Yupeng Li[a,b,c,*], Peng Zhang[a,b,c], R. Bhushan Gopaluni[d], Weihua Cao[a,b,c]

[a]*School of Automation, China University of Geosciences, Wuhan 430074, China*
[b]*Hubei Key Laboratory of Advanced Control and Intelligent Automation for Complex Systems, Wuhan 430074, China*
[c]*Engineering Research Center of Intelligent Technology for Geo-Exploration, Ministry of Education, Wuhan 430074, China*
[d]*Department of Chemical and Biological Engineering, University of British Columbia, Vancouver, BC V6T 1Z3, Canada*

Abstract

Prompt and accurate anomaly detection of drilling tools is of great significance to ensure the safe and stable operation of drilling processes. However, the operating mode of a drilling tool may often change, leading to difficulties in distinguishing the drilling anomalies from the normal mode switching. Further, the variations of drilling signals caused by such anomalies in drilling tools are usually slight, making it quite challenging to separate the abnormal part from the normal part in the time series, which would compromise the accuracy and promptness of anomaly detection. Accordingly, this paper proposes a new method for anomaly detection of drilling tools based on operating mode recognition and interval-augmented Mahalanobis distance. The main contributions are threefold: 1) A mode recognition method based on the Earth Mover's distance (EMD) and K-means clustering is proposed to identify drilling operating modes. 2) An anomaly detection method based on the interval-augmented Mahalanobis distance (IAMD) is proposed to detect anomalies of drilling tools. 3) An alarm generation strategy based on the kernel density estimation and alarm deadband is designed to reduce the false alarm rate. The effectiveness of the proposed method is demonstrated by industrial case studies involving a real drilling system.

Keywords: Drilling process, Anomaly detection, Mode recognition, Alarm optimization

1. Introduction

Drilling tools are the major equipment for resource exploration in geological drilling processes. However, due to the harsh environments and complex disturbances in the well, drilling tools may easily fall into degraded working conditions or even cause drilling accidents. According to Willersrud et al. (2015), drilling failures caused by abnormal operating time account for 20% to 25% of the total drilling time. If a drilling anomaly is not detected in time, it may develop into a serious accident. For instance, the 2010 Gulf of Mexico blowout caused by excessive pressure inside the drill pipe resulted in direct huge economic losses and serous environmental pollution (Norazahar et al., 2014). Timely identification of anomalies and adjustment of drilling strategies are essential to the safety and efficiency of drilling processes.

Commonly used anomaly detection for drilling tools includes model based methods and data-driven methods (Li et al., 2021b). The former requires the establishment of mechanism models, e.g., the axial dynamic model (Liu et al., 2022), the torsional dynamic model (Liu et al., 2019), and the transverse

dynamic model of the drilling tool (Kapitaniak et al., 2018). As the motion of drilling tools was in three-dimension, accordingly some coupled dynamic models were established, e.g., Kamel and Yigit (2014); Ding et al. (2023) applied the lumped parameter method to obtain the coupled dynamic model of the axial and torsional drilling system. In addition, dynamic models of the drill bit and rock were utilized to evaluate drilling performance (Trindade, 2020). However, the mechanism model is specific and it is difficult to adapt to changes in the formation environment, such as the formation pressure and rock type.

Data-driven methods extract features from drilling data and train classifiers to detect anomalies. In Rafezi and Hassani (2023), the wavelet packet was used to decompose vibration signals and then the back-propagation artificial neural network was exploited to detect the bit bounce and quantify the degree of bit wear. In Wang et al. (2022), the Bayesian network and the auxiliary classifier generative adversarial network were combined to construct an anomaly diagnosis model for drilling processes. In addition, an improved intelligent fault diagnosis method was proposed by Han et al. (2022) based on the moving window sparse principal component analysis; it used integrated case-based reasoning to analyze the anomaly data and determine the anomaly type. In Chamkalani et al. (2013), a mixed least square support vector machine method was developed to predict pipe adhesion. In order to identify the bit wear under different operating modes, Fan et al. (2023) designed an adaptive monitoring framework based on neighbourhood preserva-

---

*Corresponding author
Email addresses:* wenkaihu@cug.edu.cn (Wenkai Hu),
HBin@cug.edu.cn (Bin Hu), yupengli@cug.edu.cn (Yupeng Li),
zhangpengau@cug.edu.cn (Peng Zhang),
bhushan.gopaluni@ubc.ca (R. Bhushan Gopaluni),
weihuacao@cug.edu.cn (Weihua Cao)

tion embedding. To adapt to formation changes, Zhang et al. (2022) exploited historical formation data for domain invariant representation learning, so as to identify bit bounce anomalies at different depths.

The above studies provide effective solutions for anomaly detection in drilling systems. However, there are two major problems with the existing approaches: 1) Most researches aims at detecting anomalies in the drilling down mode (Yang et al., 2023; Zhang et al., 2023b), whereas the drilling operation may switch between multiple modes; thus, methods designed for a single mode cannot adapt to the mode changes and thus may generate significant false and missed alarms. 2) Improving the accuracy of anomaly detection is the major concern in existing research, while the promptness is often overlooked, which is critical for early detection of drilling anomalies (Aslam et al., 2023). Motivated by the above issues, this paper proposes a new method for anomaly detection of drilling tools based on operating mode recognition and interval-augmented Mahalanobis distance. The proposed method consists of two major stages: In the first stage, the distance between the normal time series and the reference time series in terms of data distributions is calculated and different operating modes are identified through clustering; in the second stage, monitoring indicators under different operating modes are devised and compared with the designed alarm limits to detect whether an anomaly is present. The main contributions of this paper are threefold:

1) A mode recognition method based on the Earth Mover's distance (EMD) and K-means clustering is proposed to identify drilling operating modes.

2) An anomaly detection method based on the interval-augmented Mahalanobis distance (IAMD) is proposed to detect anomalies of drilling tools.

3) An alarm generation strategy based on the kernel density estimation and alarm deadband is designed to reduce the false alarm rate.

The remainder of this paper is organized as follows: Section 2 describes the problem. Section 3 presents the proposed method for drilling anomaly detection. Section 4 demonstrates the effectiveness of the proposed method based on actual drilling examples, followed by conclusions in Section 5.

2. Problem description

Fig. 1 displays the diagram of a geological drilling system, where the top drive motor serves as a power unit to generate torque and drive the drillstring to rotate, the drillstring system pulls the bottom hole assembly (BHA) to cut and crush the rock (Fan et al., 2022), and the mud circulation system returns the cuttings and mud to the surface mud pit. In a drilling system, there are five key process variables, including the rate of penetration (ROP, m/h), weight on bit (WOB, kN), hook load (HKL, kN), rotary per minutes (RPM, r/min), and torque (TRQ, kN·m). Field operators monitor drilling operations by observing real-time trends of these variables to ensure safe drilling operations (Liu et al., 2021).

The most common anomalies in drilling tools are the bit bounce and pipe sticking. The bit bounce usually occurs when
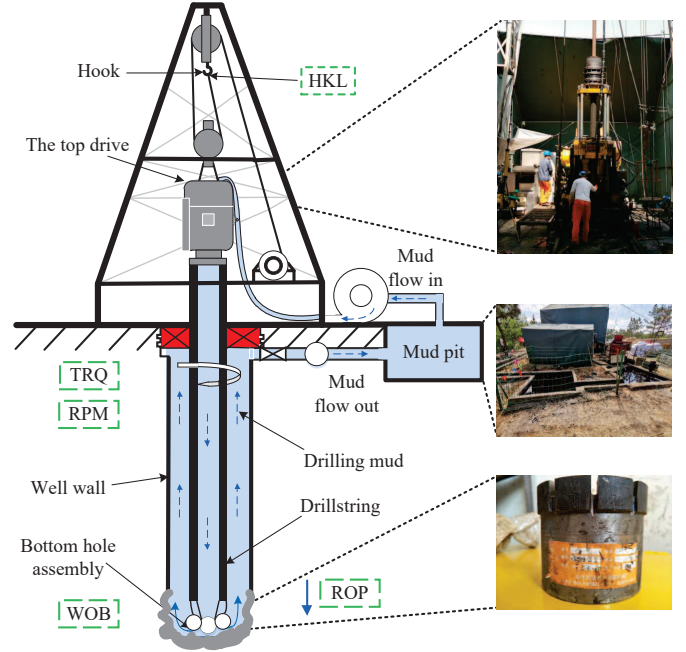

Fig. 1. Diagram of a geological drilling system.

the drill bit hits the hard formation and loses contact with the downhole formation. The pipe sticking is an issue that the drill bit and pipe are not rotating properly and it is usually caused by the unstable hole walls and loose formation in the well. If such anomalies are not handled well, the drilling tools may operate in a fatigue state for a long period, resulting in serious accidents, such as the drilling tool breakage. The difficulties in detecting the anomalies of drilling tools lie in the following two aspects:

- The operating mode of a drilling tool may often change, making the drilling variables run in several different normal operating zones, which lead to the difficulty in distinguishing the drilling anomalies from the normal mode switching. If the same alarm limits are used under different modes, it can result in massive false and missed alarms.

- As the bit bounce and pipe sticking are not as serious as real drilling accidents, the fluctuations in the drilling signals caused by them are usually slight, making it challenging to separate the abnormal part from the normal part in the time series, which would compromise the accuracy and promptness of anomaly detection.

The common operating modes of a drilling tool include the stable drilling, sweeping hole, and mode switching. Fig. 2 shows the time series of the above five variables under two operating modes, namely, the stable drilling and sweeping hole. The operating mode is switched at $t = 695$ s. It can be seen that these drilling variables show different variations under the two operating modes. Specifically, ROP shows significant variations in amplitude; WOB, HKL, RPM, and TRQ exhibit slight amplitude changes. Thus, among the five variables, ROP is the one most sensitive to mode switching and thus can be used as the key signal to distinguish operating modes. As the drilling
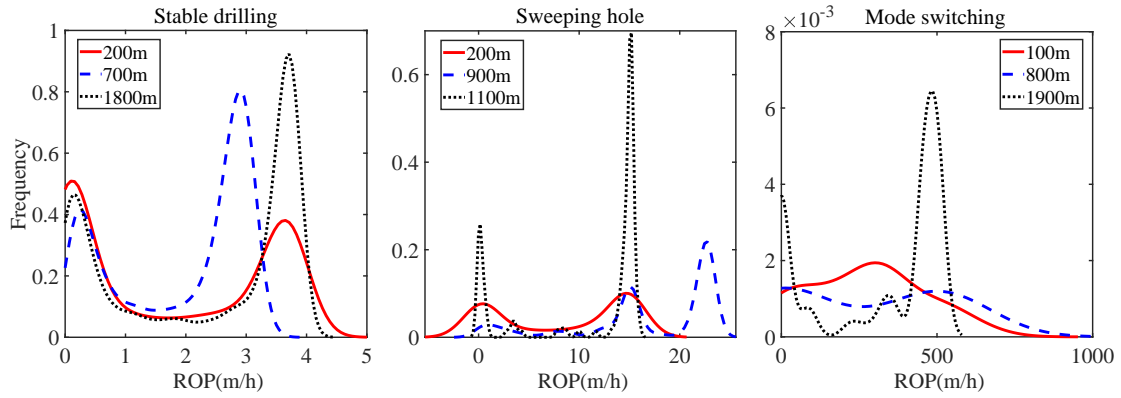
Fig. 3. Distributions of ROP at different operating modes and well depths.
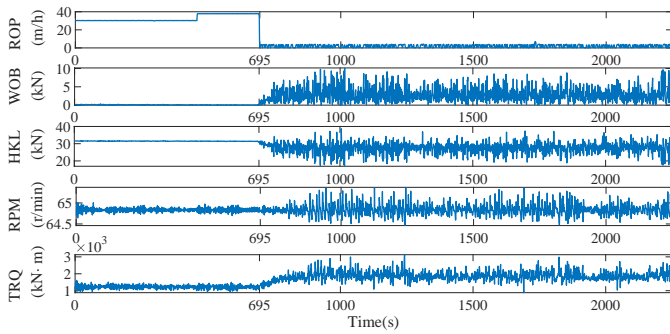

Fig. 2. Plots for ROP, WOB, HKL, RPM, and TRQ in different operating modes.

depth increases, the data distribution of the drilling signals may change. In order to verify the feasibility of using ROP to identify operating modes at different depths, Fig. 3 displays the data distribution of ROP under three different modes, namely, the stable drilling, sweeping hole, and mode switching. It can be seen that in the same mode, the variational ranges of ROP under different drilling depths are very close to each other; in different operating modes, even if the drilling depths are similar, the data distributions are quite different. Therefore, it is reasonable to choose ROP as the key drilling signal to identify operating modes. The other four drilling variables, although not sensitive to mode switching, are inextricably linked to tool operation and are thus used to monitor tool anomalies.

According to the above analysis, this paper proposes a new method with two major stages for anomaly detection of drilling tools:

1) Recognition of operating modes: Considering that the data distributions of ROP are disparate under different operating modes, the Earth Mover's distance (EMD) is used to measure the difference between the normal time series and the reference time series in terms of distributions; then, K-means clustering is applied to recognize operating modes based on the EMDs.

2) Detection of anomalies: Given the multiple drilling signals, the monitoring indicators based on the interval-augmented Mahalanobis distance is designed and the alarm generalization

strategy is developed to adapt to different operating modes.

During realtime monitoring, the current operating mode is identified by judging which cluster center the EMD of ROP is closest to, and then the Mahalanobis distance is calculated based on all the process variables and is compared with the alarm limit under the corresponding mode to determine whether an anomaly occurs. The specific implementation of the proposed anomaly detection method is described in the next section.

3. The proposed method

This section presents the proposed anomaly detection method for drilling tools, including the recognition of operating modes based on the EMD and K-means clustering, design of monitoring statistic indicator based on the IAMD, alarm limit design through kernel density estimation, and alarm performance optimization based on threshold deadband.

3.1. Recognition of operating modes

This subsection presents the method to recognize operating modes of drilling processes prior to anomaly detection. Fig. 3 shows the data distribution of ROP under three operating modes, namely, steady drilling, sweeping hole, and mode switching. It can be seen that even when the drilling depth is close, the variational ranges of ROP under the three modes overlap with each other in a large proportion, making it difficult to distinguish the two modes by directly setting a threshold. In (Li et al., 2021a), the Jensen-Shannon divergence was applied to measure the difference of data conforming to the same distribution, so as to identify operating modes. However, in geological drilling, ROP may correspond to different data distributions under different operating modes. Considering that EMD can measure the difference between the distribution of two data sets of different lengths and does not depend on the distribution hypothesis of the data, it has high flexibility in measuring different distribution differences (Zhang et al., 2023a). In this section, EMD is used to quantify differences in the distribution of ROP data for different operating modes.

Given an ROP reference data segment $\boldsymbol{x}_{r1} = [x_{r1}(1), \cdots, x_{r1}(j), \cdots, x_{r1}(n)]'$ and an ROP comparison

data segment $\boldsymbol{x}_{r2} = [x_{r2}(1), \cdots, x_{r2}(i), \cdots, x_{r2}(m)]'$ with window widths n and m, respectively, where $x_{r1}(j)$ and $x_{r2}(i)$ are the jth and ith values, respectively, in the corresponding ROP fragments. The EMD between $\boldsymbol{x}_{r2}$ and $\boldsymbol{x}_{r1}$ is then calculated as

$$\text{EMD}(\boldsymbol{x}_{r2}, \boldsymbol{x}_{r1}) = \min_{\boldsymbol{\beta}=[\beta_{ij}]} \frac{\sum_{i=1}^{m}\sum_{j=1}^{n} \varphi_{ij} \cdot \beta_{ij}}{\sum_{i=1}^{m}\sum_{j=1}^{n} \beta_{ij}} \quad (1)$$

where φ_{ij} and β_{ij} are the ordinal difference value and the value of moving from $\boldsymbol{x}_{r2}$ to $\boldsymbol{x}_{r1}$, respectively; min denotes the minimum total cost of moving from $\boldsymbol{x}_{r2}$ to $\boldsymbol{x}_{r1}$. The constraint conditions of $\text{EMD}(\boldsymbol{x}_{r2}, \boldsymbol{x}_{r1})$ are

$$\beta_{ij} \geq 0 \quad 1 \leq i \leq m, 1 \leq j \leq n \quad (2)$$

$$\sum_{j=1}^{n} \beta_{ij} \leq x_{r2}(i) \quad 1 \leq i \leq m \quad (3)$$

$$\sum_{i=1}^{m} \beta_{ij} \leq x_{r1}(j) \quad 1 \leq j \leq n \quad (4)$$

$$\sum_{i=1}^{m}\sum_{j=1}^{n} \beta_{ij} = \min\left(\sum_{i=1}^{m} x_{r2}(i), \sum_{j=1}^{n} x_{r1}(j)\right) \quad (5)$$

where Eq. (2) means that the amount moved from $x_{r2}(i)$ to $x_{r1}(j)$ is non-negative; Eq. (3) represents that the amount moved out of $x_{r2}(i)$ does not exceed itself; Eq. (4) implies that the amount moved into $x_{r1}(j)$ does not exceed itself; and Eq. (5) indicates that the total amount moved does not exceed the minimum of the total value of the data in $\boldsymbol{x}_{r2}$ and $\boldsymbol{x}_{r1}$.

According to Briani et al. (2016), the implementation of Eq. (1) is equivalent to solving the problem: $\min_{\boldsymbol{\beta}=[\beta_{ij}]} \sum_{i=1}^{m}\sum_{j=1}^{n} \varphi_{ij} \cdot \beta_{ij}$, which can be solved using linear programming

$$\begin{aligned}
\text{minimize} \quad & \boldsymbol{\varphi}^T \boldsymbol{\beta} \\
\text{subject to} \quad & \boldsymbol{A\beta} = \boldsymbol{b} \\
& \boldsymbol{\beta} \geq 0
\end{aligned} \quad (6)$$

where the cost vector $\boldsymbol{\beta} \in R^{(m \cdot n) \times 1}$, the distance vector $\boldsymbol{\varphi} \in R^{(m \cdot n) \times 1}$, the distribution vector $\boldsymbol{b} \in R^{(m+n) \times 1}$, and the coefficient matrix $\boldsymbol{A} \in R^{(m+n) \times (m \cdot n)}$ are defined as follows

$$\boldsymbol{\beta} = [\beta_{11}, \beta_{12}, \ldots, \beta_{1n}, \beta_{21}, \ldots, \beta_{2n}, \ldots, \beta_{m1}, \ldots, \beta_{mn}]' \quad (7)$$

$$\boldsymbol{\varphi} = [\varphi_{11}, \varphi_{12}, \ldots, \varphi_{1n}, \varphi_{21}, \ldots, \varphi_{2n}, \ldots, \varphi_{m1}, \ldots, \varphi_{mn}]' \quad (8)$$

$$\boldsymbol{b} = [x_{r2}(1), \cdots, x_{r2}(i), \cdots, x_{r2}(m), x_{r1}(1), \cdots, x_{r1}(j), \cdots, x_{r1}(n)]' \quad (9)$$

$$\boldsymbol{A} = \begin{bmatrix}
\mathbb{1}_n & 0 & 0 & \cdots & 0 \\
0 & \mathbb{1}_n & 0 & \cdots & 0 \\
0 & 0 & \mathbb{1}_n & \cdots & 0 \\
\vdots & \vdots & \vdots & \ddots & \vdots \\
0 & 0 & 0 & \cdots & \mathbb{1}_n \\
\boldsymbol{I}_n & \boldsymbol{I}_n & \boldsymbol{I}_n & \boldsymbol{I}_n & \boldsymbol{I}_n
\end{bmatrix} \quad (10)$$

where $\boldsymbol{I}_n$ is the identity matrix of $n \times n$ and $\mathbb{1}_n$ is an all 1 vector of $1 \times n$. The estimated value $\boldsymbol{\beta}^*$ is determined by using linear programming to solve Eq. (6) under the given constraints.

Considering the easy implementation and efficient computation of K-means (Liang et al., 2016), this clustering algorithm is applied here for mode identification based on the calculated EMDs. The K-means clustering iterates to find a cluster that minimizes the loss function denoted by

$$Loss = \sum_{j=1}^{k} \sum_{e_i \in \boldsymbol{e}} \left\| e_i - c_j \right\| \quad (11)$$

where e_i is the EMD between the ROP sequence in the P_ith window of the offline phase and the reference segment $\boldsymbol{x}_{r1}$; the vector $\boldsymbol{e}$ represents the set of obtained EMD values; c_j denotes the center of the jth cluster; k represents the number of clusters and is determined as the number of unique operating modes.

The offline clustering algorithm based on EMD and K-means is summarized in Algorithm 1. The input includes offline ROP segment $\boldsymbol{x}_{rf} \in R^{1 \times N}$, reference ROP segment $\boldsymbol{x}_{r1} \in R^{1 \times \tau}$, and the number of clusters k. The output is the cluster center c_j of each cluster C_j. In line 1, a sliding window of width v is used to intercept $\boldsymbol{x}_{rf}$ into $N - v + 1$ data segments. Line 2 calculates the EMD between different segments and $\boldsymbol{x}_{r1}$, and stores all EMDs in the vector $\boldsymbol{e}$. Lines 3 to 12 execute K-means clustering based on the EMDs. In line 3, k initial clustering centers are selected randomly; then, in lines 5 to 8, each calculated difference value e_i is assigned to the nearest cluster C_j; nest, in lines 9 to 11, k new clustering centers are obtained according to the results of the last clustering; last, in line 12, the above clustering steps are repeated until the loss function reaches a minimum value. In the online phase, the value EMD at time t is assigned to the nearest cluster C_j to determine the current operating mode.

Algorithm 1 The operating mode clustering algorithm based on EMD and K-means.

Input: $\boldsymbol{x}_{rf}, \boldsymbol{x}_{r1}, k$;
Output: center c_j of each cluster C_j;
1: $\boldsymbol{x}_{rf}$ is intercepted into $N - v + 1$ segments by a window of size v;
2: The EMDs between different segments and $\boldsymbol{x}_{r1}$ are calculated and stored in $\boldsymbol{e}$;
3: Select any k samples $c_j (j = 1, ..., k)$ in $\boldsymbol{e}$ as the initial centers, let cluster $C_j = \phi$;
4: **repeat**
5:     **for** $i = 1 : N - v + 1$ **do**
6:         $d_{ij} = \| e_i - c_j \|$;
7:         $e_i \in C_j \rightarrow \text{argmin} d_{ij}$;
8:     **end for**
9:     **for** $j = 1 : k$ **do**
10:        Calculate new cluster center $c_j = \frac{1}{C_j} \sum_{e_i \in C_j} e_i$;
11:     **end for**
12: **until** The centers c_j are not updated;

3.2. Calculation of interval-augmented Mahalanobis distance

As the variables in a drilling process usually hold high correlations with each other, ignoring such correlations in detection

4

of drilling anomalies may lead to incorrect conclusions. Accordingly, in this section, the Mahalanobis distance (MD) (Gre et al., 2021), as a distance measure incorporating correlations, is exploited to construct the monitoring statistic indicator for anomaly detection. Taking RPM and TRQ as an example in Fig. 4, where the green and blue points represent the normal samples, the purple square point represents the mean of the samples, and the red triangular point represents the abnormal sample. Here, P_x and P_y denote two directions representing the two principal components; P_{x1}, P_{y1}, P_{x2}, and P_{y2} are the projected values of the green and red triangular points in the P_x and P_y directions, respectively. Intuitively, the red triangular point is closer to the center of the mean than the blue point, but the red triangular point is an abnormal sample and the blue circle point is a normal sample. Considering that normal data tend to be distributed in the direction of the principal component P_x and components decomposed in the direction of P_y have a lower component value while abnormal samples have opposite distributions, the Mahalanobis distance is taken in this section to reduce the influence of the data trend distribution on drilling anomaly detection (Shang et al., 2018).
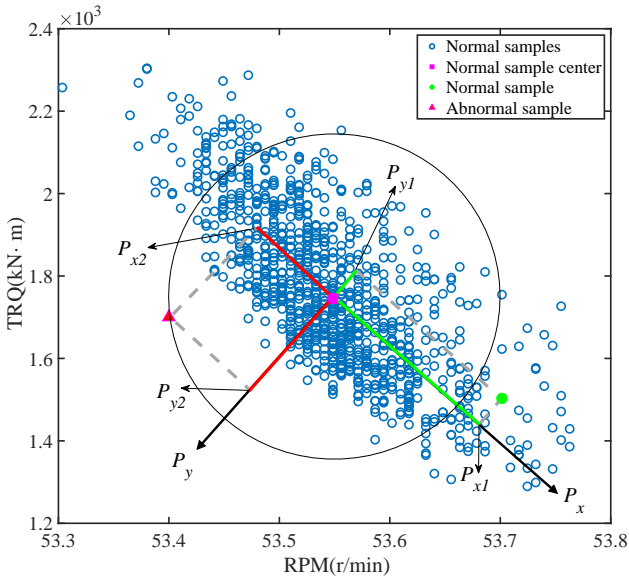

Fig. 4. Scatterplot for RPM and TRQ.

As the variations of drilling signals in the presence of a drilling anomaly are usually non-obvious, it needs to take the historical samples in a certain longer time window rather than only the current sample values. Meanwhile, there is a trade-off between the window size and the number of samples in calculation. If all data samples in a long time window are used, it may improve the detection accuracy but would also increase the computation. In view of the slight changes of drilling signals, this work proposes to make use of interval-augmented data for the calculation of Mahanobis distance. Given the time series $x(t) \in R^{1 \times M}$ of M drilling variables at time instant t, its interval-augmented vector $x_{\lambda,L}(t) \in R^{1 \times M \cdot L}$ is represented as

$$x_{\lambda,L}(t) = [x(t) \cdots x(t - \lambda(j - 1)) \cdots x(t - \lambda(L - 1))] \quad (12)$$

where λ denotes the sampling interval and L is the number of historical samples selected, i.e, the L historical samples within the time window $\lambda(L - 1)$ from the current time t are included. Accordingly, given the sample matrix $X \in R^{N \times M}$ for model training, its interval-augmented sample matrix $X_{\lambda,L} \in R^{[N + \lambda(1-L)] \times M \cdot L}$ is denoted by

$$X_{\lambda,L} = \begin{bmatrix} x(1 - \lambda(1 - L)) & \cdots & x(1 - \lambda(j - L)) & \cdots & x(1) \\ \vdots & \ddots & \vdots & \ddots & \vdots \\ x(t) & \cdots & x(t - \lambda(j - 1)) & \cdots & x(t - \lambda(L - 1)) \\ \vdots & \ddots & \vdots & \ddots & \vdots \\ x(N) & \cdots & x(N - \lambda(j - 1)) & \cdots & x(N - \lambda(L - 1)) \end{bmatrix}$$
(13)

where N is the number of samples used in model training.

For the interval-augmented vector $x_{\lambda,L}(t)$ at time t, the interval-augmented Mahanobis distance (IAMD) statistic $d_{\lambda,L}(t)$ is calculated as

$$d_{\lambda,L}(t) = \sqrt{(x_{\lambda,L}(t) - \mu_{\lambda,L}) \Sigma_{\lambda,L}^{-1} (x_{\lambda,L}(t) - \mu_{\lambda,L})^T} \quad (14)$$

where $\Sigma_{\lambda,L}$ is the covariance matrix of the interval-augmented matrix $X_{\lambda,L}$; $\Sigma_{\lambda,L}^{-1}$ represents the inverse matrix of $\Sigma_{\lambda,L}$; $\mu_{\lambda,L} = \begin{bmatrix} \mu_1 & \cdots & \mu_j & \cdots & \mu_{M \cdot L} \end{bmatrix}'$ represents the column mean vector of the matrix $X_{\lambda,L}$, and μ_j denotes the mean of the data in column j of $X_{\lambda,L}$. The covariance matrix $\Sigma_{\lambda,L}$ is given by

$$\Sigma_{\lambda,L} = \begin{bmatrix} \text{Cov}(a_1, a_1) & \cdots & \text{Cov}(a_1, a_i) & \cdots & \text{Cov}(a_1, a_{M \cdot L}) \\ \vdots & \ddots & \vdots & \ddots & \vdots \\ \text{Cov}(a_i, a_1) & \cdots & \text{Cov}(a_i, a_i) & \cdots & \text{Cov}(a_i, a_{M \cdot L}) \\ \vdots & \ddots & \vdots & \ddots & \vdots \\ \text{Cov}(a_{M \cdot L}, a_1) & \cdots & \text{Cov}(a_{M \cdot L}, a_i) & \cdots & \text{Cov}(a_{M \cdot L}, a_{M \cdot L}) \end{bmatrix}$$
(15)

where $M \cdot L$ denotes the column count of $X_{\lambda,L}$; $\text{Cov}(a_i, a_j)$ represents the covariance between any two dimensions or columns a_i and a_j in $X_{\lambda,L}$ as (Li and Zhu, 2023)

$$\text{Cov}(a_i, a_j) = \frac{1}{N + \lambda(1 - L) - 1} \sum_{t=1}^{N + \lambda(1-L)} (a_i(t) - \mu_{a_i})(a_j(t) - \mu_{a_j})$$
(16)

where $N + \lambda(1 - L)$ denotes the number of rows in $X_{\lambda,L}$; $a_i(t)$ and $a_j(t)$ are the tth values in a_i and a_j, respectively; μ_{a_i} and μ_{a_j} represent the mean values of the a_i and a_j vectors, respectively.

3.3. Alarm generation strategy

Given the calculated IAMD in Eq. (14), it needs to compare it with an alarm limit, so as to determine whether the drilling process is under a normal or anomalous state. This subsection presents an alarm generation strategy for drilling anomaly detection based on IAMD statistics. The IAMD statistic is the sum of squares of variables with many degrees of freedom and the Chi-squared distribution is used to fit the MD statistic in the Ji et al. (2019). However, the interval-augmented MD statistic does not always satisfy the hypothesis of Chi-squared distribution, and the fitting effect of Chi-squared distribution may not be satisfactory (Corina and Hovda, 2018). Accordingly, this subsection adopts the kernel density estimation (KDE) to fit the

IAMD statistics under different values of λ and L. The KDE function $f_{\lambda,L}^h(x)$ is given by

$$f_{\lambda,L}^h(x) = \frac{1}{[N + \lambda(1-L)]h} \sum_{t=1-\lambda(1-L)}^{N} K\left(\frac{d_{\lambda,L}(t) - x}{h}\right) \quad (17)$$

where x represents the value of the continuous IAMD, h is the bandwidth of the kernel function, $d_{\lambda,L}(t)$ denotes the IAMD for tth sample in the training data, and $K(\cdot)$ stands for the Gaussian kernel function given by

$$K\left(\frac{d_{\lambda,L}(t) - x}{h}\right) = \frac{1}{\sqrt{2\pi}} \exp\left[-\frac{1}{2}\left(\frac{d_{\lambda,L}(t) - x}{h}\right)^2\right] \quad (18)$$

where exp represents the exponential function.

The alarm limit $A_{\lambda,L}$ is inversely calculated from the integral of the probability distribution function

$$\delta = \int_{-\infty}^{A_{\lambda,L}} f_{\lambda,L}^h(x) dx \quad (19)$$

where δ is the confidence level.

Eventually, during online monitoring phase, the value of the IAMD statistic $d_{\lambda,L}(t)$ for realtime samples is compared with the value of the designed alarm limit $A_{\lambda,L}$ to determine the alarm state $a(t)$, i.e.,

$$a(t) = \begin{cases} 1 & d_{\lambda,L}(t) \geq A_{\lambda,L} \\ 0 & d_{\lambda,L}(t) < A_{\lambda,L} \end{cases} \quad (20)$$

where $a(t) = 1$ indicates that the drilling process is under an anomalous state at time t; otherwise, the process is normal and no alarm is generated.

Due to the complex geological environment, the drilling signals are easily disturbed by the external disturbances during the drilling process, resulting in high false and missed alarm rates. It is therefore necessary to improve the alarm generation strategy in anomaly detection. An effective way is the alarm deadband, which is widely used to optimize alarm configuration in process industries (Afzal et al., 2018; Gyasi and Wang, 2022). By designing a suitable alarm deadband, the false and missed alarms can be effectively reduced. Thereby, the alarm generation strategy in Eq. (20) is improved by designing an alarm deadband. The alarm signal $a(t)$ with an alarm deadband is formulated as

$$a(t) = \begin{cases} 1 & \text{if } d_{\lambda,L}(t) \geq A_{\lambda,L} + \omega/2 \\ 0 & \text{if } d_{\lambda,L}(t) < A_{\lambda,L} - \omega/2 \\ a(t-1) & \text{otherwise} \end{cases} \quad (21)$$

where ω denotes the width of the designed alarm deadband.

Fig. 5 gives an illustrative example of an alarm deadband. Fig. 5(a) shows the plot of the monitoring statistics (blue curve), the fixed alarm limit (dashed red line), and the deaband (green rectangle); Fig. 5(b) gives the alarm signal based on a fixed alarm limit and Fig. 5(c) presents the alarm signal based on the alarm deadband. Under normal circumstances, the alarm signal should be generated continuously during time period [a,

g]. However, under the fixed threshold in Fig. 5(b), because the monitoring statistic traverse the fixed alarm limit, it is detected that no anomaly has occurred during periods (c, d) and (e, f), which increases the missed alarm rate and also caused alarm repeating for three times. With the alarm deadband, the alarm signal in Fig. 5(c) is continuously generated during [b, h]. Compared to Fig. 5(b), there may be a small increase in detection delay within an acceptable range, but it significantly reduces the false alarm rate and improves the accuracy of the alarm system.
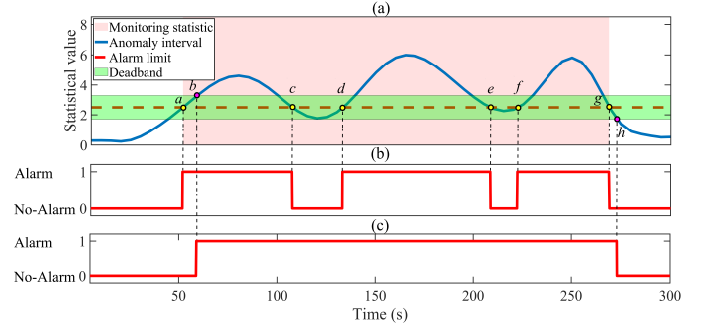

Fig. 5. An example of an alarm deadband.

3.4. Procedures and Performance Evaluation

This subsection summarizes the steps of the proposed anomaly detection method using a diagram shown in Fig. 6. The main steps for the offline part are as follows:

Step 1 - Clustering for different operating modes: Given the historical ROP data x_{rf}, and then the sliding window is used to intercept x_{rf} and the data segment set of x_{rf} is obtained. The EMDs between different segments and x_{r1} are calculated based on Eq. (1) to get the set e, and then K-means clustering is used to determine the clustering centers corresponding to different operating modes.

Step 2 - Design of IAMD alarm limits and deadbands: Given the historical data X of the drilling variables over the same time period of x_{rf}, data augmentation is conduced to obtain $X_{\lambda,L}$ based on Eq. (13). Meanwhile, the mean $\mu_{\lambda,L}$ and covariance $\Sigma_{\lambda,L}$ of $X_{\lambda,L}$ are also calculated. Then, the IAMD is calculated based on Eq. (14) for each sample, and KDE is used to facilitate the design of alarm limit $A_{\lambda,L}$ and deadband ω under different operating modes.

From the offline calculation, the clustering centers c_j, mean vector $\mu_{\lambda,L}$, covariance matrix $\Sigma_{\lambda,L}$, alarm limit $A_{\lambda,L}$, and alarm deadband ω are determined and used in the online monitoring stage. The main steps of the online part are as follows:

Step 1 - Operating mode recognition: Given the online window data segment $x_{rn}(t)$ at the current time t, and then the EMD $e_n(t)$ is calculated based on Eq. (1). The K-means assigns the $e_n(t)$ to the cluster with the closest operating mode center.

Step 2 - Online anomaly detection: At the current time instant t, the interval-augmented data $x_{\lambda,L}^*(t)$ is obtained, the I-AMD $d_{\lambda,L}^*(t)$ is calculated by Eq. (14) based on $\mu_{\lambda,L}$ and $\Sigma_{\lambda,L}$ of the associated operating mode. The alarm signal $a^*(t)$ is generated by Eq. (21) based on the designed alarm limit $A_{\lambda,L}$ and

6

deadband ω; if it is detected $a^*(t) = 1$, a drilling anomaly is detected to be present.
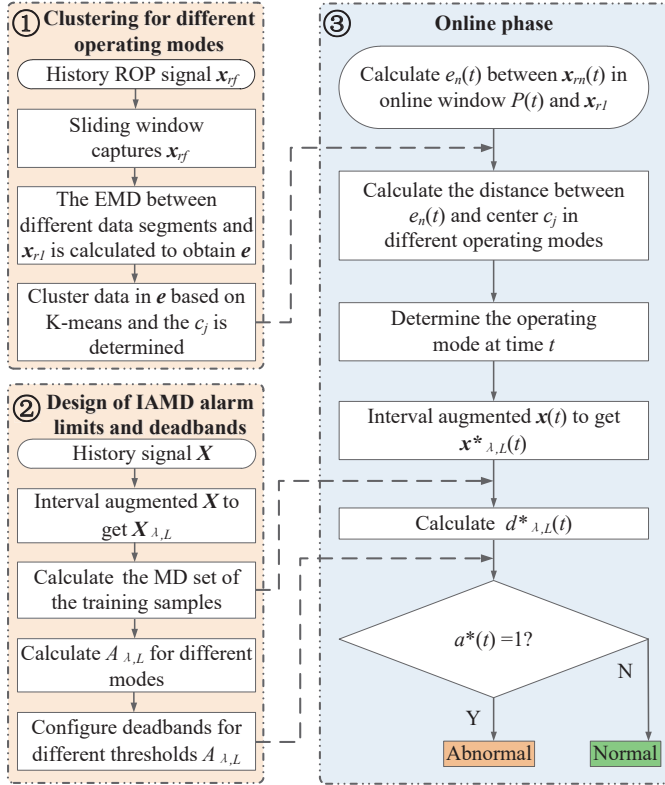

Fig. 6. The diagram for the offline calculation and online monitoring of the proposed method.

To compare the anomaly detection performance of the method, performance metrics including the accuracy (Acc), the false alarm rate (FAR), and the missed alarm rate (MAR) are used, i.e.,

$$\text{Acc} = \frac{T_P + T_N}{T_P + T_N + F_P + T_N} \tag{22}$$

$$\text{FAR} = \frac{F_P}{F_P + T_N} \tag{23}$$

$$\text{MAR} = \frac{F_N}{T_P + F_N} \tag{24}$$

where T_P, F_N, F_P, T_N stand for the number of true positives, false negatives, false positives, and true negatives, respectively. In addition, the Detection Delay (DD) is also exploited to assess the detection promptness. The DD refers to the time from the occurrence of an anomaly to the presence of the alarm. Smaller values of FAR, MAR, and DD, or a larger Acc, indicate better performance of the anomaly detection scheme; vice versa.

In the calculation of the IAMD, there are two key adjustment parameters, namely, the time interval λ for data augmentation and the number L of augmented samples, which may have significant influences to the anomaly detection result. Accordingly, this works adopts the Technique for Order Preference by Similarity to Ideal Solution (TOPSIS) method to screen out the best evaluation effect of the two parameters (Atenidegbe and

Mogaji, 2023); the calculation process is summarized as follows:

Set the test ranges of λ and L as $[1, \lambda^{\text{max}}]$ and $[1, L^{\text{max}}]$, respectively. Under each combination of λ and L, the metrics Acc, FAR, MAR, and DD are calculated. Denote the number of parameter combinations as $z = \lambda^{\text{max}} \cdot L^{\text{max}}$, a matrix for the performance metrics is obtained as

$$\overline{\chi}_{\text{Ind}} = \begin{bmatrix} \overline{\eta}_{\text{Acc}} & \overline{\eta}_{\text{MAR}} & \overline{\eta}_{\text{FAR}} & \overline{\eta}_{\text{DD}} \end{bmatrix} \in R^{z \times 4} \tag{25}$$

where $\overline{\eta}_{\text{Acc}}$, $\overline{\eta}_{\text{MAR}}$, $\overline{\eta}_{\text{FAR}}$, and $\overline{\eta}_{\text{DD}}$ denote the vectors consisting of Acc, MAR, FAR, and DD under z combinations of λ and L .

As MAR, FAR, and DD have opposite changing directions compared to Acc, the conversion is conducted as

$$\begin{cases} \widehat{\eta}_{\text{MAR}} &= \max(\overline{\eta}_{\text{MAR}}) - \overline{\eta}_{\text{MAR}} \\ \widehat{\eta}_{\text{FAR}} &= \max(\overline{\eta}_{\text{FAR}}) - \overline{\eta}_{\text{FAR}} \\ \widehat{\eta}_{\text{DD}} &= \max(\overline{\eta}_{\text{DD}}) - \overline{\eta}_{\text{DD}} \end{cases} \tag{26}$$

where max() is the largest element in the index vector. Then, there is $\widehat{\chi}_{\text{Ind}} = [\overline{\eta}_{\text{Acc}}, \widehat{\eta}_{\text{MAR}}, \widehat{\eta}_{\text{FAR}}, \widehat{\eta}_{\text{DD}}]$.

To ensure the reliability of the results, it is necessary to standardize the metrics. The standardization process is given by

$$\begin{cases} \eta_{\text{Acc}} &= \overline{\eta}_{\text{Acc}}/\|\overline{\eta}_{\text{Acc}}\|_2 \\ \eta_{\text{MAR}} &= \widehat{\eta}_{\text{MAR}}/\|\widehat{\eta}_{\text{MAR}}\|_2 \\ \eta_{\text{FAR}} &= \widehat{\eta}_{\text{FAR}}/\|\widehat{\eta}_{\text{FAR}}\|_2 \\ \eta_{\text{DD}} &= \widehat{\eta}_{\text{DD}}/\|\widehat{\eta}_{\text{DD}}\|_2 \end{cases} \tag{27}$$

where $\|\cdot\|_2$ denotes the l_2 norm. Then, the matrix for the performance metrics is $\chi_{\text{Ind}} = [\eta_{\text{Acc}}, \eta_{\text{MAR}}, \eta_{\text{FAR}}, \eta_{\text{DD}}]$.

Based on the matrix χ_{Ind}, a comprehensive index ψ is calculated; ψ denotes a weighted value of the four metrics. Each element of ψ is given by

$$\psi_i = \frac{D_i^-}{D_i^+ + D_i^-}, i = 1, 2, \cdots, z \tag{28}$$

where D_i^+ and D_i^- are calculated as

$$D_i^+ = \sqrt{\sum_{j=1}^4 \xi_j [\chi_{\text{Ind}}(i, j) - \max(\chi_{\text{Ind}}(:, j))]^2} \tag{29}$$

$$D_i^- = \sqrt{\sum_{j=1}^4 \xi_j [\chi_{\text{Ind}}(i, j) - \min(\chi_{\text{Ind}}(:, j))]^2} \tag{30}$$

where ξ_j is the weight of the jth index; here, the metrics are weighted equally, i.e., $\xi_j = 1$. Eventually, the maximum value of ψ is obtained as the final comprehensive index used to evaluate the influence of λ and L.

4. Industrial Case Studies

This section demonstrates the effectiveness of the proposed anomaly detection method based on case studies with data collected from a real geothermal drilling site in China. The data includes 4175 samples during normal operation involving three

operating modes. Fig. 7 displays the time series of four drilling variables. The period from 1 s to 2000 s was corresponding to the stable drilling, the sweeping hole was from 2001 s to 3800 s, and the mode switching occured from 3801 s to 4175 s. As discussed in Section 2, the ROP is exploited in operating mode recognition and the other four variables are used for anomaly detection.
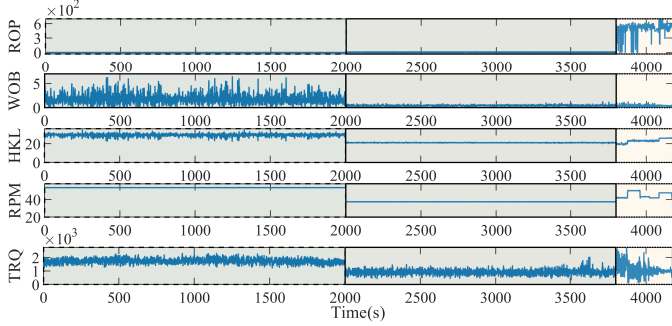

Fig. 7. Time series of ROP, WOB, HKL, RPM, and TRQ under three different operating modes.

In the actual drilling process, the stable drilling mode occupies most of the total drilling time. Therefore, the ROP data under stable drilling is taken as the reference data distribution x_{r1} for operating mode detection. The ROP fragments under different modes are captured by a sliding window of width $v = 30$, and the step size is set to 1. Then, the EMDs between the fragments in the sliding window and x_{r1} are calculated. After that, K-means clustering is applied to cluster the data based on the calculated EMDs. Considering that there are three different modes, the number of clusters is set to be $k = 3$. Fig. 8 displays the calculated EMDs in subplot (a) and the clustering results in subplot (b). Each cluster is associated with an operating mode. The centers of these clusters are obtained as $c_1 = 7.2148$, $c_2 = 470.3043$, and $c_3 = 0.2897$.
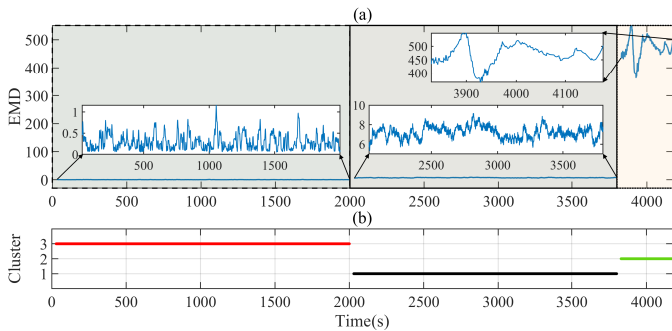

Fig. 8. EMD calculation and clustering results in offline phase.

Next, two cases are presented to illustrate the anomaly detection using the proposed method. The alarm limits under different modes are designed by the KDE method; the alarm deadband for the IAMD statistics is set to 20% of the statistical value. Meanwhile, some other classic anomaly detection methods are applied for comparison, including the Principal Component Analysis (PCA) (Zhang et al., 2021), standard Mahalanobis

Distance (MD) (Yang and Delpha, 2022), and Kullback-Leibler Divergence (KLD) (Li et al., 2021c).

4.1. Case 1

This case involves detection of bit bounce. In the real drilling process, the drill bit drilled into the dolomite with an uneven texture, resulting in the bit bounce. Fig. 9 shows the time series of all the drilling variables, where the red curves denote the period under the bit bounce from 727 s to 1029 s.
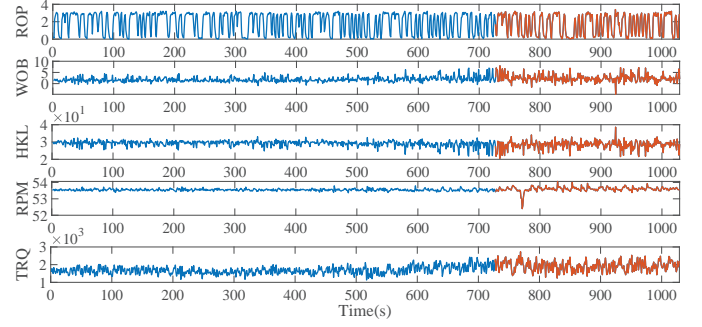

Fig. 9. Time series of ROP, WOB, HKL, RPM, and TRQ under the bit bounce in Case 1.
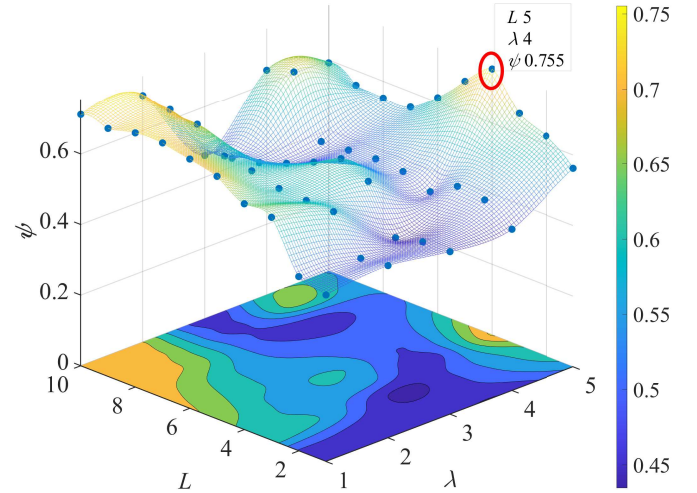

Fig. 10. Comprehensive index under different combinations of λ and L in Case 1.

Simulations are conducted to evaluate the influence of λ and L, which are set as $\lambda = 1 \sim 5$ and $L = 1 \sim 10$. Thus, there are $z = 50$ different combinations of λ and L. Fig. 10 shows the plot of the calculated comprehensive index under different λ and L using the TOPSIS method in Section 3.4. The blue point highlighted by a red ellipse represents the best performance achieved with $\lambda = 5$ and $L = 4$. Thus, in the rest of Case 1, this pair of parameters is used in the calculation of I-AMD.

Fig. 11 shows the anomaly detection results using both the proposed method and other comparison methods. For each method, there is a subplot presenting the trend of the monitoring statistics (blue curve) and the corresponding alarm signal
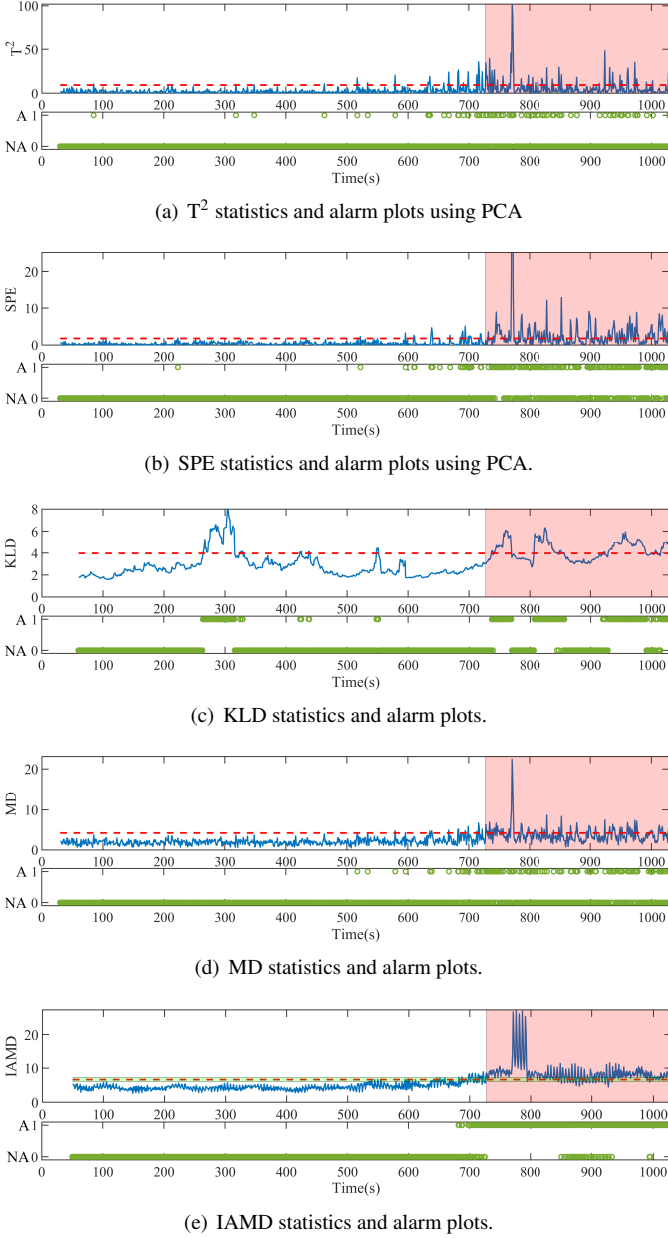
(a) T^2 statistics and alarm plots using PCA

(b) SPE statistics and alarm plots using PCA.

(c) KLD statistics and alarm plots.

(d) MD statistics and alarm plots.

(e) IAMD statistics and alarm plots.

Fig. 11. Anomaly detection results in Case 1.

Table 1 Comparison of different methods in Case 1; − indicates that the method fails in anomaly detection.

Method		PCA (T^2)	PCA (SPE)	KLD	MD	IAMD
Without operating mode recognition	Acc(%)	71.20	70.80	69.30	70.30	71.23
	FAR(%)	6.03	0.57	2.01	1.43	1.45
	MAR(%)	81.19	95.05	96.70	94.72	91.09
	DD(s)	−	−	−	−	−
With operating mode recognition	Acc(%)	72.70	82.10	79.28	77.00	**94.39**
	FAR(%)	3.01	3.01	9.45	2.44	**3.25**
	MAR(%)	83.17	52.15	45.54	70.30	**10.89**
	DD(s)	−	16	13	−	**0**

nition. In the scenario without mode recognition, the normal drilling is considered. It can be observed from the table that all the methods fail to detect the drilling anomaly when the mode recognition is not conducted. With mode recognition, the anomaly detection performance metrics for all the methods are improved; specifically, the SPE of PCA, KLD, and the proposed method based on IAMD achieve successful anomaly detection. Comparing the performance metrics of difference methods in the scenario with mode recognition, it can be seen that the proposed method based on IAMD outperforms all the other approaches significantly; its anomaly detection accuracy is as high as 94.39% and the detection delay is 0.

4.2. Case 2

This case involves detection of pipe sticking under the sweeping hole operating mode. Fig. 12 shows the time series of the five drilling variables. The pipe sticking happened over the period from 216 s to 359 s. It can be observed that these variables exhibited different variations in the presence of pipe sticking; there were slight increases in WOB and TRQ, a minor decrease in HKL, and a slow fluctuation in RPM.
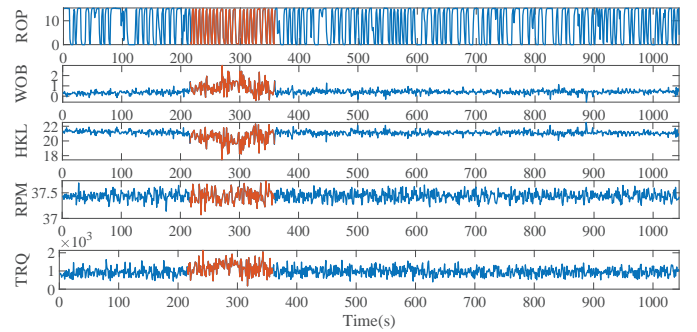

Fig. 12. Time series of ROP, WOB, HKL, RPM, and TRQ under the bit bounce in Case 2.

Fig. 13 presents the plot of the calculated comprehensive index using the TOPSIS method in Section 3.4. It can be observed that the best performance is achieved at the blue point with $\lambda = 1$ and $L = 7$, as highlighted by a red ellipse. Accordingly, in the rest of Case 2, this pair of parameters is used in the calculation of IAMD.
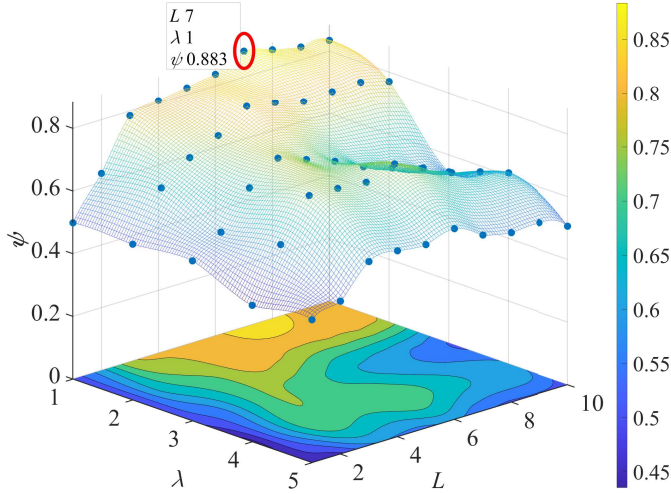
(green circles). The red dashed line represents the calculated alarm limit for each statistical index; the symbol NA and A in the alarm lots indicate the non-alarm state and alarm state, respectively. It can be observed from Fig. 11(a) and (b) that the T^2 and SPE of PCA fluctuate around the alarm limits during the bit bounce, resulting in a large number of missed alarms. The same problem can also be observed with the original MD statistics in Fig. 11(d). As for the KLD statistic in Fig. 11(c), it can be seen that the FAR is rather high as shown during the normal operating period around 300 s. In contrast, the proposed method has very low false and missed alarm rates as shown in Fig. 11(e).

Table 1 summarizes the performance metrics of all the methods in two scenarios without and with operating mode recog-

Fig. 13. Comprehensive index under different combinations of λ and L in Case 2.

Fig. 14 displays the anomaly detection results using both the proposed method and other comparison methods. It can be observed from Fig. 14(a), (b) and (d) that the T^2 and SPE statistics of PCA, as well as the original MD statistics, have high missed alarm rates during the period of pipe sticking. From Fig. 14(c), it can be seen that the KLD has a lower missed alarm rate but much larger detection delay. In contrast, the proposed method achieved a smaller detection delay, as well as much lower false and missed alarm rates, as shown in Fig. 14(e).

Table 2 Comparison of different methods in Case 2; − indicates that the method fails in anomaly detection.

Method		PCA (T²)	PCA (SPE)	KLD	MD	IAMD
Without operating mode recognition	Acc(%)	85.91	87.68	85.62	85.81	85.80
	FAR(%)	0.00	0.92	0.23	0.00	0.00
	MAR(%)	99.31	81.25	1.00	1.00	1.00
	DD(s)	−	−	−	−	−
With operating mode recognition	Acc(%)	86.21	87.98	92.98	91.82	**96.83**
	FAR(%)	0.00	3.21	0.00	4.02	**3.70**
	MAR(%)	97.22	65.28	48.61	33.33	**0.00**
	DD(s)	−	−	28	53	**0**

Table 2 summarizes the performance metrics of all the methods in two scenarios without and with operating mode recognition. It can be observed that without mode recognition, all the methods fail in detecting the drilling anomaly. Incorporating the operating mode recognition, KLD, MD, and the proposed method based on IAMD succeed in anomaly detection. Thus, it can be concluded that the the proposed mode recognition method based on EMD and K-means can effectively identify the correct operating mode, which is helpful in the further detection of drilling anomaly. Comparing the performance metrics of different methods in the scenario with operating mode recognition, it can be observed that the proposed method based on IAMD achieves more excellent performance with the detec-
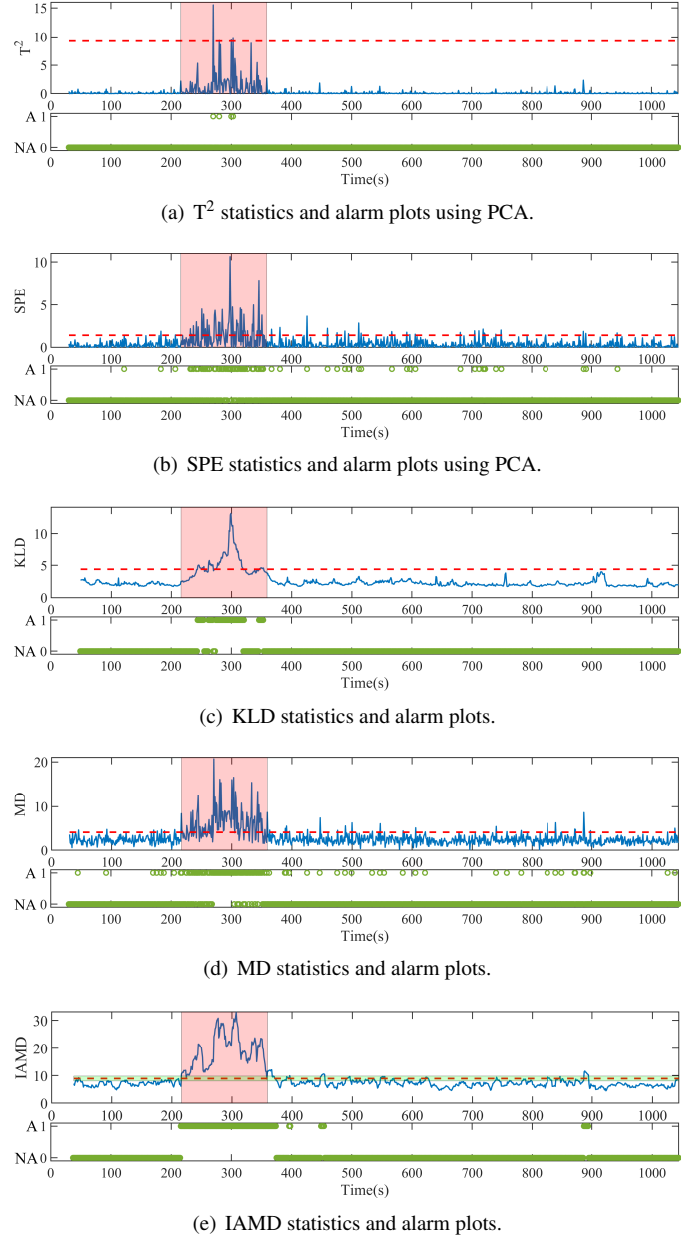

(a) T^2 statistics and alarm plots using PCA.

(b) SPE statistics and alarm plots using PCA.

(c) KLD statistics and alarm plots.

(d) MD statistics and alarm plots.

(e) IAMD statistics and alarm plots.

Fig. 14. Anomaly detection results in Case 2.

tion accuracy as 96.83% and the detection delay as 0, which are much better than the metrics using KLD and MD.

5. Conclusion

To improve the accuracy and promptness of anomaly detection in drilling tools, this paper proposes a new method based on operating mode recognition and interval-augmented Mahalanobis distance. The proposed method consists of two major stages. First, an operating mode recognition method based the Earth Mover's distance and K-means clustering is proposed to identify operating modes of the drilling process. Then, the anomaly detection is achieved by calculating the interval-augmented Mahalanobis distance (IAMD) and design-

ing the alarm generation strategy. The results in the industrial case studies demonstrated that the proposed anomaly detection method detected the drilling anomalies correctly and achieved much higher detection accuracy and lower detection delay compared to other state-of-the-art methods.

Acknowledgements

References

Afzal, M.S., Chen, T., Bandehkhoda, A., Izadi, I., 2018. Analysis and design of time-deadbands for univariate alarm systems. Control Engineering Practice 71, 96–107.

Aslam, A.M., Aseel, A., Rithul, R., Pranav, S., 2023. Predictive big data analytics for drilling downhole problems: A review. Energy Reports 9, 5863–5876.

Atenidegbe, O.F., Mogaji, K.A., 2023. Modeling assessment of groundwater vulnerability to contamination risk in a typical basement terrain using topsis-entropy developed vulnerability data mining technique. Heliyon 9, e18371.

Briani, M., Cristiani, E., Iacomini, E., 2016. Sensitivity analysis of the lwr model for traffic forecast on large networks using wasserstein distance. Communications in Mathematical Sciences 16.

Chamkalani, A., Pordel Shahri, M., Poordad, S., 2013. Support vector machine model: A new methodology for stuck pipe prediction. SPE Middle East Unconventional Resources Conference and Exhibition , SPE–164003–MS.

Corina, A., Hovda, S., 2018. Automatic lithology prediction from well logging using kernel density estimation. Journal of Petroleum Science and Engineering 170, 664–674.

Ding, S., Fang, P., Li, G., Lu, J., Wang, Y., Li, Y., Han, Y., Xiao, D., 2023. Axial-torsional nonlinear vibration of bottom hole assembly in the air drilling technology. Petroleum .

Fan, H., Lu, C., Lai, X., Du, S., Yu, W., Wu, M., 2023. Adaptive monitoring for geological drilling process using neighborhood preserving embedding and jensen-shannon divergence. Control Engineering Practice 134, 105476.

Fan, H., Wu, M., Lai, X., Du, S., Yu, W., Lu, C., 2022. A decentralized operating performance assessment for geological drilling process via multi-block total projection to latent structures and bayesian inference. Journal of Process Control 117, 26–39.

Gre, S., Dhler, M., Mevel, L., 2021. Hankel matrix-based mahalanobis distance for fault detection robust towards changes in process noise covariance. IFAC-PapersOnLine 54, 73–78. 19th IFAC Symposium on System Identification SYSID 2021.

Gyasi, P., Wang, J., 2022. Design of serial alarm systems based on deadbands and delay timers for removing false alarms. Process Safety and Environmental Protection 162, 1033–1041.

Han, Y., Liu, J., Liu, F., Geng, Z., 2022. An intelligent moving window sparse principal component analysis-based case based reasoning for fault diagnosis: Case of the drilling process. ISA Transactions 128, 242–254.

Ji, H., Huang, K., Zhou, D., 2019. Incipient sensor fault isolation based on augmented mahalanobis distance. Control Engineering Practice 86, 144–154.

Kamel, J.M., Yigit, A.S., 2014. Modeling and analysis of stick-slip and bit bounce in oil well drillstrings equipped with drag bits. Journal of Sound and Vibration 333, 6885–6899.

Kapitaniak, M., Vaziri, V., Pez Chvez, J., Wiercigroch, M., 2018. Experimental studies of forward and backward whirls of drill-string. Mechanical Systems and Signal Processing 100, 454–465.

Li, W., Zhu, J., 2023. Clt for spiked eigenvalues of a sample covariance matrix from high-dimensional gaussian mean mixtures. Journal of Multivariate Analysis 193, 105127.

Li, Y., Cao, W., Hu, W., Wu, M., 2021a. Abnormality detection for drilling processes based on jensenshannon divergence and adaptive alarm limits. IEEE Transactions on Industrial Informatics 17, 6104–6113.

Li, Y., Cao, W., Hu, W., Wu, M., 2021b. Identification of downhole conditions in geological drilling processes based on quantitative trends and expert rules. Neural Computing and Applications .

Li, Y., Cao, W., Hu, W., Xiong, Y., Wu, M., 2021c. Incipient fault detection for geological drilling processes using multivariate generalized gaussian distributions and kullbackleibler divergence. Control Engineering Practice 117, 104937.

Liang, H., Sun, Y., Li, G., Li, Z., 2016. Gray relational clustering model for intelligent guided monitoring horizontal wells. Neural Computing and Applications 31, 1339–1351.

Liu, J., Ma, X., Zhang, X., Zhang, Z., Liu, G., 2022. Axial vibration of deep-water drilling risers under lifting conditions. Journal of Petroleum Science and Engineering 209, 109903.

Liu, Y., Lin, W., Pez Chvez, J., De Sa, R., 2019. Torsional stick-slip vibrations and multistability in drill-strings. Applied Mathematical Modelling 76, 545–557.

Liu, Z., Ma, Q., Cai, B., Liu, Y., Zheng, C., 2021. Risk assessment on deepwater drilling well control based on dynamic bayesian network. Process Safety and Environmental Protection 149, 643–654.

Norazahar, N., Khan, F., Veitch, B., MacKinnon, S., 2014. Human and organizational factors assessment of the evacuation operation of bp deepwater horizon accident. Safety Science 70, 41–49.

Rafezi, H., Hassani, F., 2023. Drill bit wear monitoring and failure prediction for mining automation. International Journal of Mining Science and Technology 33, 289–296.

Shang, J., Chen, M., Zhang, H., 2018. Fault detection based on augmented kernel mahalanobis distance for nonlinear dynamic processes. Computers & Chemical Engineering 109, 311–321.

Trindade, M.A., 2020. Robust evaluation of stability regions of oil-well drilling systems with uncertain bit-rock nonlinear interaction. Journal of Sound and Vibration 483, 115481.

Wang, C., Ma, J., Jin, H., Wang, G., Chen, C., Xia, Y., Gou, J., 2022. Acgan and bn based method for downhole incident diagnosis during the drilling process with small sample data size. Ocean Engineering 256, 111516.

Willersrud, A., Blanke, M., Imsland, L., Pavlov, A., 2015. Fault diagnosis of downhole drilling incidents using adaptive observers and statistical change detection. Journal of Process Control 30, 90–103.

Yang, A., Lu, C., Yu, W., Hu, J., Nakanishi, Y., Wu, M., 2023. Data augmentation considering distribution discrepancy for fault diagnosis of drilling process with limited samples. IEEE Transactions on Industrial Electronics 70, 11774–11783.

Yang, J., Delpha, C., 2022. An incipient fault diagnosis methodology using local mahalanobis distance: Detection process based on empirical probability density estimation. Signal Processing 190, 108308.

Zhang, J., Xiao, C., Yang, W., Liang, X., Zhang, L., Wang, X., 2023a. Probabilistic geothermal resources assessment using machine learning: Bayesian correction framework based on gaussian process regression. Geothermics 114, 102787.

Zhang, J., Zhou, D., Chen, M., 2021. Monitoring multimode processes: A modified pca algorithm with continual learning ability. Journal of Process Control 103, 76–86.

Zhang, W., Meng, X., Zhang, W., Zhu, J., Chen, G., 2023b. Dynamic risk assessment of deepwater drilling using data-based and probabilistic approach. Ocean Engineering 268, 113414.

Zhang, Z., Lai, X., Lu, C., Du, S., Yu, W., Wu, M., 2022. Bit bounce detection and alarm optimization based on domain generalization for drilling process. IEEE Transactions on Instrumentation and Measurement 71, 1–11.